

Article

# Synthesis, Characterization and Wettability of Cu-Sn Alloy on the Si-Implanted 6H-SiC

Xiang Zhao Zhang <sup>1</sup>, Pu Hao Xu <sup>1</sup>, Gui Wu Liu <sup>1,2,\*</sup>, Awais Ahmad <sup>3</sup> , Xiao Hui Chen <sup>1,2</sup>,  
Ya Long Zhu <sup>1</sup>, Asma Alothman <sup>4,\*</sup> , Shahid Hussain <sup>1,\*</sup>  and Guan Jun Qiao <sup>1</sup>

<sup>1</sup> School of Materials Science and Engineering, Jiangsu University, Zhenjiang 212013, China; xzzhang2018@ujs.edu.cn (X.Z.Z.); 13667004282@163.com (P.H.X.); chenxiaohui058@163.com (X.H.C.); 18852897590@163.com (Y.L.Z.); gjqiao@ujs.edu.cn (G.J.Q.)

<sup>2</sup> School of Mechanical and Electrical Engineering, Xinyu University, Xinyu 338000, China

<sup>3</sup> Department of Chemistry, The University of Lahore, Lahore 54590, Pakistan; awaisahmed@gcuf.edu.pk

<sup>4</sup> Department of Chemistry, College of Science, King Saud University, Riyadh 11451, Saudi Arabia

\* Correspondence: gwliu76@ujs.edu.cn (G.W.L.); aalothman@ksu.edu.sa (A.A.); shahid@ujs.edu.cn (S.H.)

Received: 22 August 2020; Accepted: 14 September 2020; Published: 21 September 2020



**Abstract:** The wettability of the metal/SiC system is not always excellent, resulting in the limitation of the widespread use of SiC ceramic. In this paper, three implantation doses of Si ions ( $5 \times 10^{15}$ ,  $1 \times 10^{16}$ ,  $5 \times 10^{16}$  ions/cm<sup>2</sup>) were implanted into the 6H-SiC substrate. The wetting of Cu-(2.5, 5, 7.5, 10) Sn alloys on the pristine and Si-SiC were studied by the sessile drop technique, and the interfacial chemical reaction of Cu-Sn/SiC wetting couples was investigated and discussed. The Si ion can markedly enhance the wetting of Cu-Sn on 6H-SiC substrate, and those of the corresponding contact angles ( $\theta$ ) are raised partly, with the Si ion dose increasing due to the weakening interfacial chemical reactions among four Cu-Sn alloys and 6H-SiC ceramics. Moreover, the  $\theta$  of Cu-Sn on (Si-)SiC substrate is first decreased and then increased from  $\sim 62^\circ$  to  $\sim 39^\circ$ , and  $\sim 70^\circ$  and  $\sim 140^\circ$ , with the Sn concentration increasing from 2.5%, 5% and 7.5% to 10%, which is linked to the reactivity of Cu-Sn alloys and SiC ceramic and the variation of liquid-vapor surface energy. Particularly, only a continuous graphite layer is formed at the interface of the Cu-10Sn/Si-SiC system, resulting in a higher contact angle ( $>40^\circ$ ).

**Keywords:** 6H-SiC; Cu-Sn alloy; ion implantation; wettability; interface

## 1. Introduction

Silicon carbide (SiC) has been widely applied in the field of electronics industries and metal-ceramic composites, due to its sublime properties such as high strength, high modulus, high melting point and erosion resistance [1–3]. In fact, good wettability between liquid metals and SiC ceramic plays a vital role in these areas. Up to now, two critical challenges for the SiC applications are the low wettability and the undesired interfacial reaction of metals and SiC ceramic [4]. Commonly, the equilibrium value of  $\theta$ , used to explore the wetting behavior of liquid on a flat and chemically homogeneous solid surface, observes the traditional Young's equation [5]  $\cos\theta = \sigma_{SV} - \sigma_{SL}/\sigma_{LV}$  (where  $\sigma_{SV}$  and  $\sigma_{LV}$  describe the surface tension of the solid and liquid, respectively, and the  $\sigma_{SL}$  defines the solid/liquid interfacial energy). Based on this equation, two leading technologies can be performed to reduce the  $\theta$  of metal on the SiC substrate.

One is increasing the  $\sigma_{SV}$  by changing the SiC surface (i.e., the ion implantation, Ref. [6] sintering metallization [7,8] and plasma pulses [9]. Compared with other surface modification technologies, ion implantation is a non-thermal and non-equilibrium process, where no new interface is introduced and the surface crystal structure can be altered in this process [10]. Recently, our group has proved

that Mo, Ref. [11] Pd [12] and Si [13] ion implantation can increase the  $\sigma_{SV}$  of 6H-SiC monocrystal substrate by producing lattice imperfections and point defects, and thus the ion implantation is regarded as one of the key factors affecting the wettability of Al, Ref. [13] Al-Cu and [13] Al-Si-(Cu, Mg or Zn) [6,12] on SiC monocrystal substrate. For instance, Zhu et al. [13] studied the wetting of Al-Cu/Si-implanted SiC wetting couples, indicating that the contact angles of Al-Cu alloys on Si-SiC substrates were raised partly with an increase of the Si ion dose, and the Si ion can evidently improve the wetting of Cu-Al/SiC when the content of Al is no more than 42.9% in Cu.

Another is adding elements such as (Ti, Ref. [14,15] Cr, Ref. [16] Ni [17]) into the metal to reduce the  $\sigma_{SL}$  by enhancing the interfacial interactions of metal/SiC systems and/or to simultaneously reduce the  $\sigma_{LV}$ . For the pure Cu/SiC system, a high contact angle was detected due to the formation of the graphite layer at the wetting interface [18]. Various elements such as Al [13], Si [18], and Zr [19] were added into Cu to adjust the wettability of the Cu/SiC system. As reported by Zhou et al. [19], excellent wettability ( $\theta \approx 5^\circ$ ) was observed in the Cu-Zr/SiC system at 1200 °C, and the interfacial reaction layer was transformed from a graphite layer to metallic ZrC and Zr<sub>2</sub>Si compounds after adding Zr into Cu. Furthermore, the other elements added into the pure metal can also bring about the changes of heat transfer performance compared with the pure metal [20–22], which can significantly affect the thermodynamic and kinetics of the chemical reaction between molten metal and ceramic during the wetting process. Therefore, the wettability of metal/ceramic system is further influenced accordingly.

As discussed above, both the surface modification of SiC and other metal element additions are the most promising methods to improve the wetting of metal/SiC systems. However, the influence of Sn addition on the wettability of the Cu/6H-SiC system was rarely reported, especially for the 6H-SiC ceramic after Si ion implantation. Herein, Si ion was implanted into the 6H-SiC monocrystal substrate, and the wettability of Cu-(2.5, 5, 7.5, 10) Sn (all in at.% in this text) alloys on 6H-SiC monocrystal substrate were investigated. We found that the Si ion can markedly enhance the wetting of Cu-Sn on 6H-SiC substrate, and the  $\theta$  of Cu-Sn on (Si-)SiC substrate basically decreases first, and then increases alongside the Sn concentration.

## 2. Experimental Details

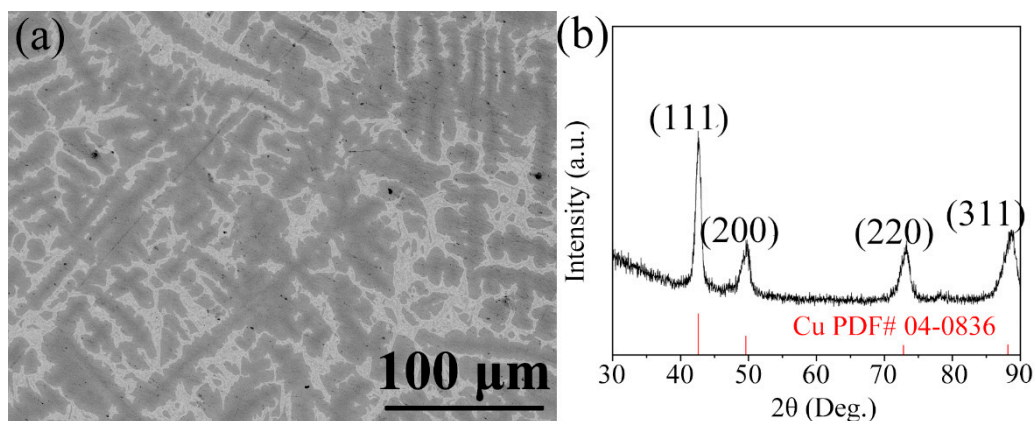
The double polished C-terminated 6H-SiC monocrystal (CAS: 409-21-2), with sizes of 10 mm × 10 mm × 0.33 mm, was employed as the wetting substrate. The Cu-(2.5, 5, 7.5, 10)Sn alloys used for the wetting experiments were fabricated by arc melting with non-consumable tungsten electrode under a purified Ar (99.99%, CAS: 7440-37-1) atmosphere, and being remelted five times to ensure a uniform composition, combining appropriate amounts of the Cu sheet (99.9 wt.% purity, CAS: 7440-50-8) and Sn granular (99.8 wt.% purity, CAS: 7440-31-5). In order to prevent the oxygen contamination, a Ti getter (CAS: 7440-32-6) was melted first, before the Cu-Sn alloy. The microstructure and phase composition of a typical Cu-7.5Sn alloy were analyzed and identified by scanning electron microscopy (SEM, FEI NovaNano450, back-scattered electron (BSE) mode) and X-ray diffraction (XRD). The scanning range of XRD examination was 20°–90°, with a speed of 5°/min. The Cu-Sn alloys featured a wire electrode cutting into the block, with sizes of 3 mm × 3 mm × 3 mm, which were carefully cleaned in acetone and ethanol successively before wetting experiments. The ion implantation was carried out in an ion implanter (MEVVA-36), and three doses of Si ions ( $5 \times 10^{15}$ ,  $1 \times 10^{16}$ ,  $5 \times 10^{16}$  ions/cm<sup>2</sup>) were implanted into the 6H-SiC substrate at 20 keV at an ambient temperature under the vacuum of  $\sim 5 \times 10^{-3}$  Pa.

The sessile drop tests of Cu-Sn alloys on a Si-implanted SiC substrate were performed at a contact angle computing instrument (OCA15LHT-SV, Dataphysics, Filderstadt, Germany). The wetting samples were performed at 1373 K for 240 min in a vacuum of  $\sim 6 \times 10^{-4}$  Pa, with a heating rate of 5 K/min. After wetting experiments, the cross-sectioned wetting systems were polished using diamond polishing fluid, and the interfacial microstructure was observed by SEM (BSE mode), coupled with energy dispersive spectroscopy (EDS). It was noted that the images obtained from BSE mode can be used to evidently present the composition contrast for the polished samples, while the images

obtained from the secondary electron (SE) model mainly reflect the contrasting information of the surface geometry.

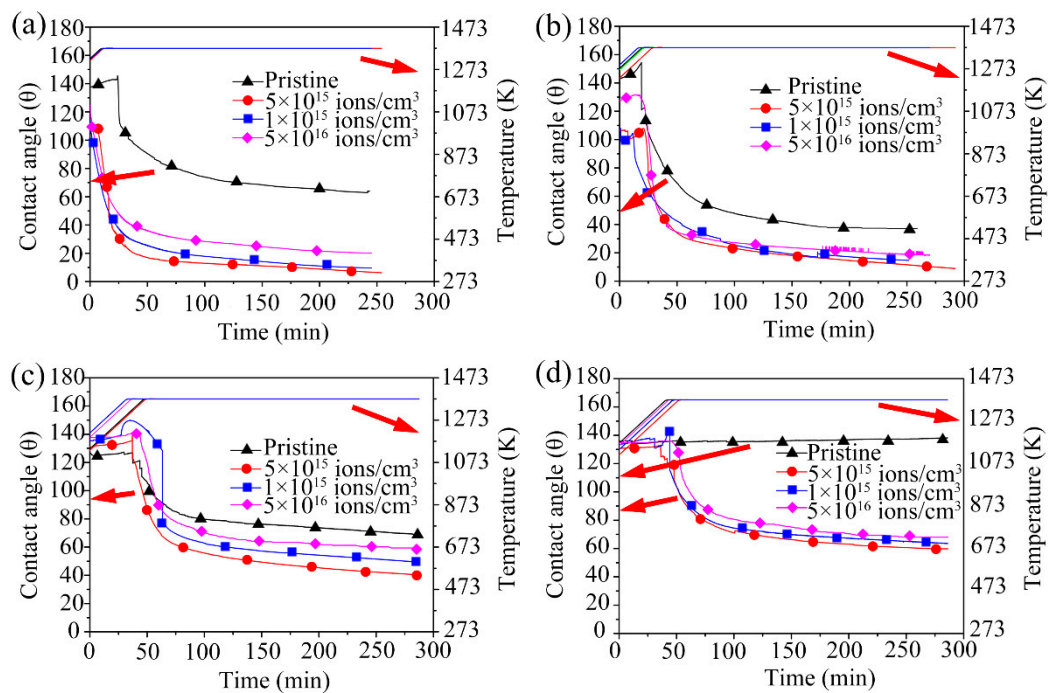
### 3. Results and Discussion

Figure 1 shows the typical microstructure of Cu-7.5Sn alloy combined with its XRD pattern. The Cu-7.5Sn alloy presents a typical dendritic microstructure, and is composed of two phases (dark and grey phase). Based on the EDS analysis, both phases are mainly Cu-rich solid solutions, where the Sn concentration in the grey phase is higher than that in the dark phase. According to the Cu-Sn binary phase diagram [23], the dark and grey phases can be confirmed as a Cu-rich solid solution (Cu) and (Cu) plus Cu-Sn compounds. However, only the (Cu) phase emerges in the XRD pattern due to the low content of the Cu-Sn compound (Figure 1b).



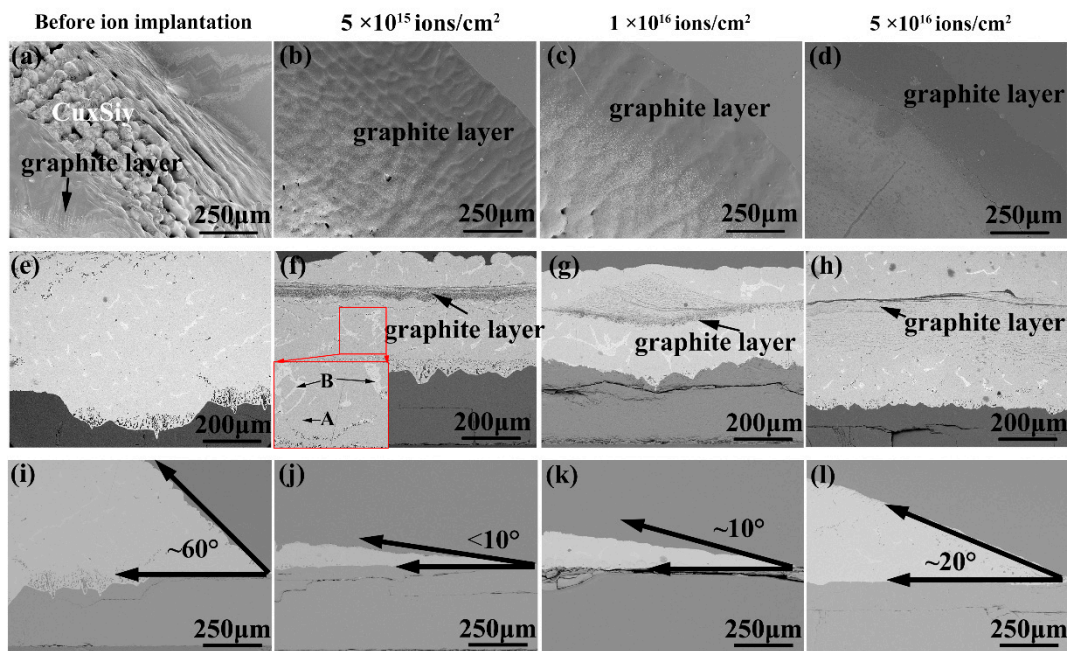
**Figure 1.** (a) Back-scattered electron (BSE) image; and (b) X-ray diffraction (XRD) pattern of Cu-7.5Sn alloy.

Figure 2 shows the wetting curves of molten Cu-(2.5, 5, 7.5, 10) Sn alloys on the (Si-)SiC substrates at 1373 K. In Figure 2, two Y-axes are drawn to present the information of the contact angle (the Y-axis on the left). The temperature (the Y-axis on the right) in Figure 2a–d and the line corresponding to the wetting temperature is 1373 K, showing a straight line in the figure. For the Cu-Sn/pristine SiC systems, the contact angle ( $\theta$ ) is first decreased, and then increased from  $\sim 62^\circ$  to  $\sim 39^\circ$  and  $\sim 70^\circ$ , with the Sn concentration rising from 2.5% to 5% and 7.5%. In particular, a non-wetting phenomenon with a high contact angle of  $\sim 140^\circ$  is observed in the Cu-10Sn/SiC system. On the other hand, the Si ion implantation has a pleasurable influence on the wetting of Cu-Sn/SiC couples. The  $\theta$  of Cu-Sn on the Si-SiC substrate decreases markedly after Si ion implantation, especially for the Cu-10Sn/Si-SiC systems transforming from non-wetting to wetting. However, the  $\theta$  of Cu-Sn/Si-SiC systems is increased partly with the Si ion dose increase, rising up to  $5 \times 10^{16}$  ions/cm<sup>2</sup>. Those experimental results illustrate that the Si ion can blatantly improve the wettability of Cu-Sn/SiC systems. In contrast, a higher Si ion dose can weaken this phenomenon, showing an increased contact angle. In these cases, the  $\sigma_{SV}$  keeps invariant (before ion implantation), or is increased due to the presence of the lattice imperfection and point defects after ion implantation [13], while the  $\sigma_{LV}$  is decreased with the Sn concentration increasing, according to Amore's results [24]. Theoretically speaking, the increased  $\sigma_{SV}$  or/and decreased  $\sigma_{LV}$  can reduce the wettability of Cu-Sn/(Si-)SiC systems based on Young's equation. Thus, the abnormally increased contact angle with the rise of the Si ion dose can be ascribed to the increased  $\sigma_{LV}$  derived from the decreasing interfacial interactions between Cu-Sn alloys and Si-SiC ceramic.



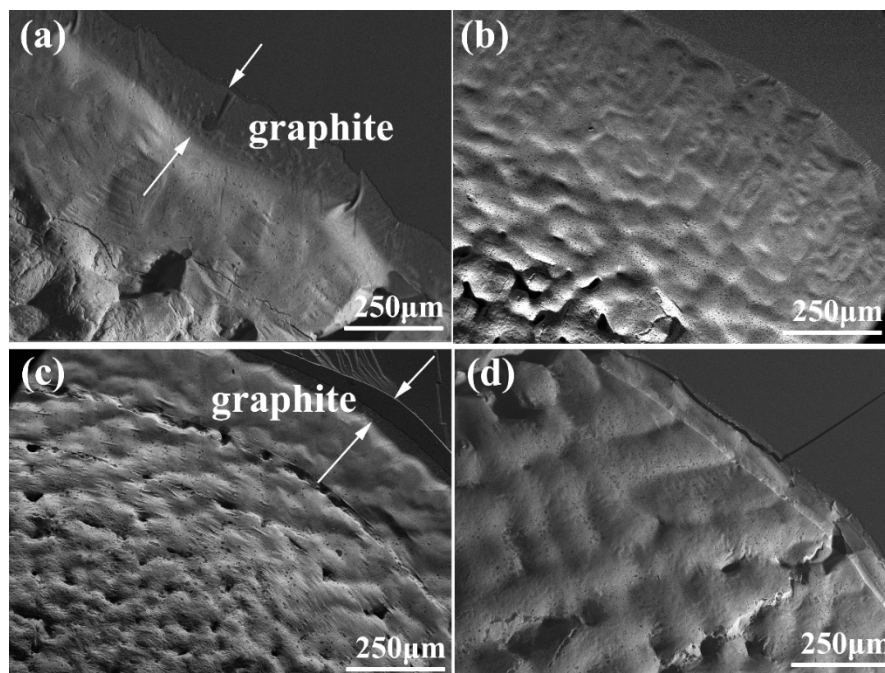
**Figure 2.** Curves of Cu-Sn/SiC systems before and after Si ion implantation ( $5 \times 10^{15}$ ,  $1 \times 10^{16}$  and  $5 \times 10^{16}$  ions/cm<sup>2</sup>) at 1373 K: (a) Cu-2.5Sn; (b) Cu-5Sn; (c) Cu-7.5Sn; and (d) Cu-10Sn.

Figure 3 shows the interfacial BSE images of Cu-2.5Sn/SiC couples before and after Si ion implantation. From Figure 3a, a prominent graphite layer and numerous  $\text{Cu}_x\text{Si}_y$  compounds are formed at the surface of Cu-2.5Sn solidified drop due to the serious chemical reaction between Cu and SiC, which is also observed in the pure Cu and SiC systems [13]. After Si ion implantation, a visible graphite film can be observed at the triple line region, and its width decreases with the Si ion dose increasing (Figure 3b–d). Moreover, a laminated graphite layer is located on the upper part of the Cu-2.5Sn drop after Si ion implantation, as shown in Figure 3f–h. The laminated graphite layer gradually becomes thin, with the Si ion implantation dose rising, indicating that the interfacial interactions are weakened, resulting in an increase of  $\sigma_{SL}$  and a contact angle, either more or less (as shown in Figures 2 and 3i–l). Meanwhile, the 6H-SiC substrate is more or less consumed with the formation of uneven scallops (Figure 3e–h). Similarly, the solidified Cu-2.5Sn drop consists of a dark phase marked A and a small amount of grey phase marked B, as shown in the insert image in Figure 3f. Based on the EDS results, the chemical compositions of the two phases are 92.09Cu + 5.90Si + 2.01Sn and 66.48Cu + 33.52Sn, respectively. According to the Cu-Si and Cu-Sn binary phase diagrams [23,25], the dark and grey phases can be confirmed as Cu-rich solid solutions, containing few Cu-Si and Cu-Sn compounds, respectively.



**Figure 3.** BSE images of Cu-2.5Sn/(Si-)SiC systems (a,e,i) before and (b–d,f–h,j–l) after Si ion implantation: (a–d) at the triple line region, cross-section (e–h) at the central interfaces and (j–l) at the triple line region.

Figures 4 and 5 exhibit the top-view and interfacial BSE images of Cu-(5, 7.5)Sn/Si-SiC systems with different Si ion implantation doses, respectively. From Figure 4a,c, a thin graphite film emerges at the triple line region of Cu-(5, 7.5)Sn/Si-SiC systems after the Si ion implantation dose of  $5 \times 10^{15}$  ions/cm<sup>2</sup>. However, a higher Si ion implantation dose ( $5 \times 10^{16}$  ions/cm<sup>2</sup>) cannot induce the formation of the graphite layer in Cu-(5, 7.5)Sn/Si-SiC systems (Figure 4b,d).



**Figure 4.** BSE images of (a,b) Cu-5Sn/Si-SiC and (c,d) Cu-7.5Sn/Si-SiC systems at the triple line region after Si ion implantation of (a,c)  $5 \times 10^{15}$  and (b,d)  $5 \times 10^{16}$  ions/cm<sup>2</sup>.

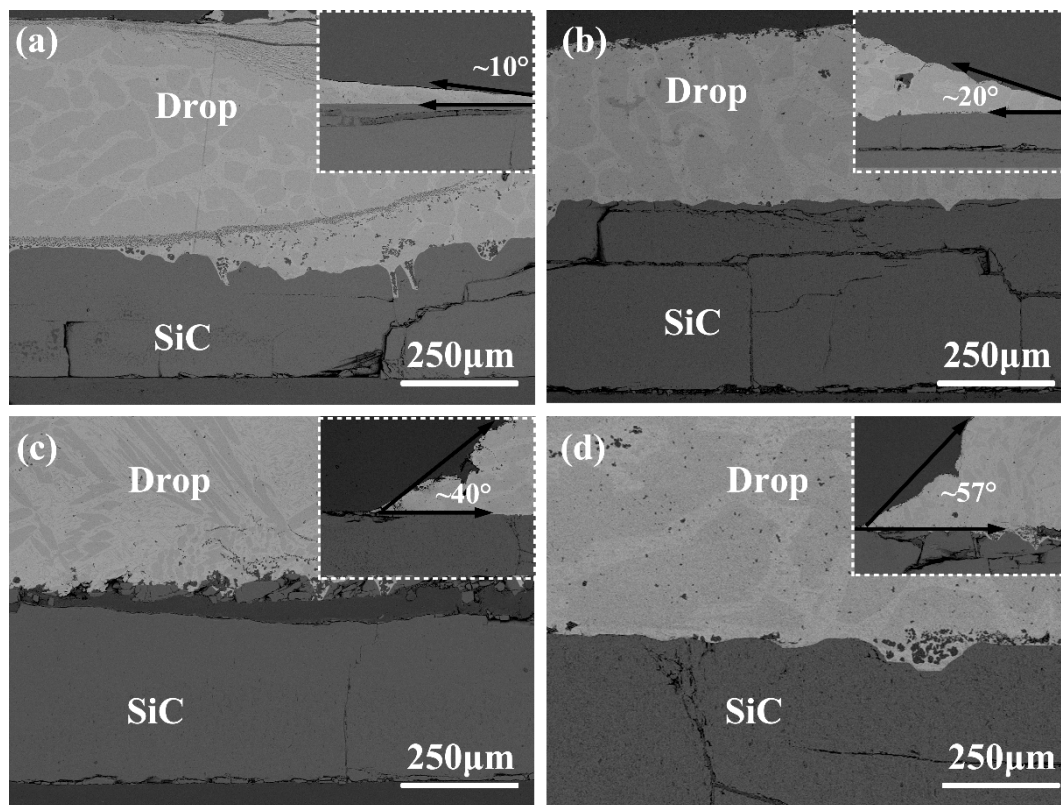


**Figure 5.** Interfacial BSE images of (a,b) Cu-5Sn/Si-SiC and (c,d) Cu-7.5Sn/Si-SiC systems at the central interfaces after Si ion implantation of (a,c)  $5 \times 10^{15}$  and (b,d)  $5 \times 10^{16}$  ions/cm<sup>2</sup>.

Compared to the Cu-2.5Sn/Si-SiC system, the Cu-(5, 7.5) Sn/Si-SiC presents relatively weak interfacial reactions, and the formed graphite layer moves closer to the SiC substrate (Figure 5). This phenomenon is mainly attributed to the low activity of Cu, due to the relatively high concentration of the Sn element. As we know, the wettability of Cu-Sn/Si-SiC couple can be comprehensively determined by the  $\sigma_{SL}$  originating from interfacial interactions, and the  $\sigma_{LV}$  on the condition of the same substrate. In these cases, the increase in  $\sigma_{SL}$  and the decrease of  $\sigma_{LV}$  correspondingly dominates the Cu-5Sn/Si-SiC and Cu-7.5Sn/Si-SiC systems, so the  $\theta$  of Cu-Sn/Si-SiC decreases firstly, and then increases, with the Sn concentration rising from 2.5% to 7.5%. Similarly, two kinds of phases (Figure 5) are also observed in the solidified Cu-(5, 7.5) Sn alloy drops, and the content of grey phase increases gradually (Figures 3–5). Accordingly, the Sn concentration in the grey phase is also raised.

Figure 6 exhibits the interfacial microstructure of Cu-10Sn/Si-SiC systems after Si ion implantation. Compared with Cu-(2.5, 5, 7.5) Sn/Si-SiC systems, the Cu-10Sn/Si-SiC presents relatively high contact angles (Figure 2). However, it is puzzling that the molten Cu-10Sn alloy has the lowest surface energy among the four Cu-Sn alloys, and thus theoretically the Cu-10Sn/Si-SiC systems should present excellent wettability, according to Young's equation. From Figure 6, only a continued graphite layer is closely attached to the SiC substrate, which is due to the fact that the high Sn concentration in Cu alloys can reduce the activity of Cu element, and thus the chemical reaction is limited at the interface. According to the reactive production control (RPC) model [26,27], wetting in the reactive system is predominated by the final interfacial production at the interface and triple region. Because the molten drop has a poor wettability on the graphite layer, there is relatively poor wettability of Cu-10Sn on Si-SiC substrates. Moreover, the interfacial chemical reaction between Cu-10Sn and Si-SiC becomes weaker and weaker as the Si ion dose rises, resulting in a thinner graphite layer and higher contact angle.

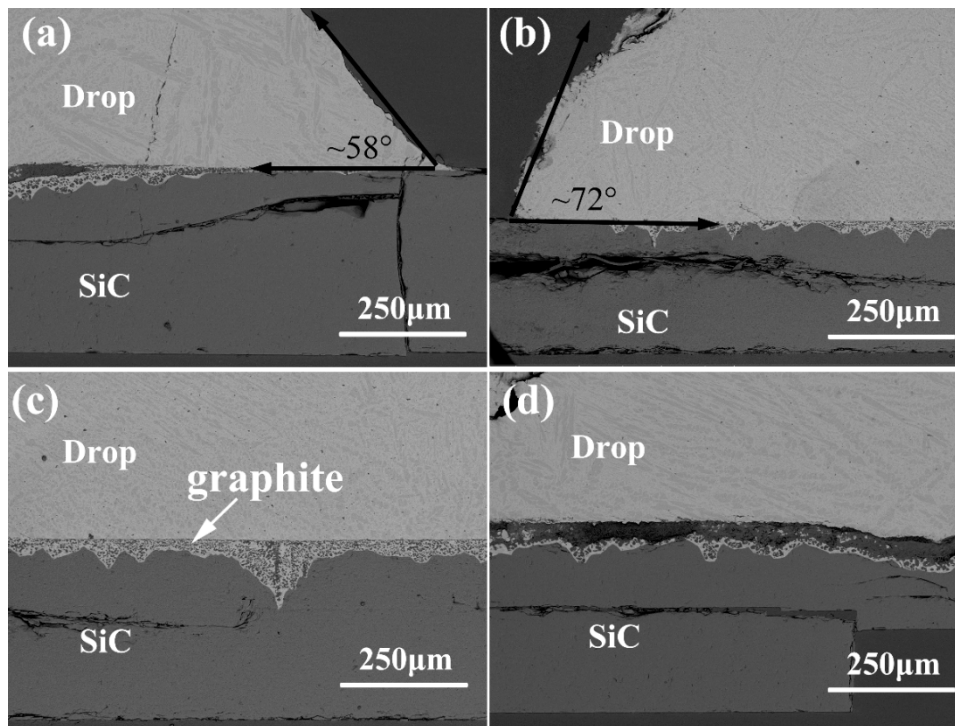


**Figure 6.** Interfacial BSE images of Cu-10Sn/SiC systems after the Si ion implantation of (a,c)  $5 \times 10^{15}$  and (b,d)  $5 \times 10^{16}$  ions/cm<sup>2</sup>.

#### 4. Conclusions

The wetting of molten Cu-(2.5, 5, 7.5, 10) Sn on Si-implanted SiC substrates was studied, and the effects of Si ion doses and Sn concentration in Cu alloys on the wettability were analyzed. The Si ion can markedly enhance the wetting of Cu-Sn/SiC systems; however, the contact angle of Cu-Sn on Si-SiC substrate partly increases, with the Si implantation dose increasing from  $5 \times 10^{15}$  to  $5 \times 10^{16}$  ions/cm<sup>2</sup>. The wetting of Cu-Sn/(Si-)SiC systems is closely related to the increasing solid-liquid interfacial energy originated from the decreasing interfacial chemical reaction and the decreasing liquid-vapor surface energy, with the Sn concentration increasing from 2.5%, 5% and 7.5% to 10%. In particular, a higher Sn concentration of  $\geq 7.5\%$  can obviously reduce the activity of Cu, resulting in a relatively weak interfacial reaction and a higher contact angle ( $>40^\circ$ ). The above work and conclusions provide a novel way to change the surface properties of ceramic and improve the wettability of the metal/SiC ceramic system, which can further expand the prospective application area of SiC ceramic. However, changes of the surface state of SiC after ion implantation in an atomic scale, i.e., the ion site in SiC lattice and the lattice distortion of SiC, were less straightforward. In the future, the first-principle calculations based on density functional theory (DFT) and *Ab-initio* molecular dynamics (AIMD) simulation can be performed to study the changes in atomic scale after the ion implantation.

**Author Contributions:** Conceptualization, X.Z.Z. and A.A. (Awais Ahmad); methodology, A.A. (Asma Alothman), P.H.X., and X.Z.Z.; software, S.H.; validation, A.A. (Awais Ahmad) and S.H.; formal analysis, S.H.; investigation, G.J.Q.; resources, A.A. (Asma Alothman); data curation, G.W.L.; writing—original draft preparation, A.A. (Awais Ahmad); writing—review and editing, visualization, X.H.C.; supervision, S.H.; project administration, Y.L.Z.; funding acquisition, X.H.C. All authors have read and agreed to the published version of the manuscript.

**Funding:** This work was funded by the Researchers Supporting Project Number (RSP-2020/243) King Saud University, Riyadh, Saudi Arabia; National Key R&D Program of China (2017YFB0310400); the National Natural Science Foundation of China (51572112); the National Natural Science Foundation of Jiangxi (20192BAB206009, 20192BAB206030); the Key Research and Development Plan (BE2019094); the Six Talent Peaks Project (TD-XCL-004); 333 talents project (BRA2017387); and the Qing Lan Project ([2016]15) of Jiangsu Province providing financial support.

**Conflicts of Interest:** The authors declare no conflict of interest.

## References

1. Fitriani, P.; Septiadi, A.; Hyuk, J.D.; Yoon, D.H. Joining of SiC monoliths using a thin MAX phase tape and the elimination of joining layer by solid-state diffusion. *J. Eur. Ceram. Soc.* **2018**, *38*, 3433–3440. [[CrossRef](#)]
2. Liu, J.W.; Zhou, X.B.; Tatarko, P.; Yuan, Q.; Huang, Q. Fabrication, microstructure, and properties of SiC/Al<sub>4</sub>SiC<sub>4</sub> multiphase ceramics via an in-situ formed liquid phase sintering. *J. Adv. Ceram.* **2020**, *9*, 193–203. [[CrossRef](#)]
3. Zhang, W.; Yamashita, S.; Kita, H. Progress in tribological research of SiC ceramics in unlubricated sliding—A review. *Mater. Des.* **2020**, *190*, 108528. [[CrossRef](#)]
4. Pervaiz, M.; Ahmad, I.; Yousaf, M.; Kirn, S.; Munawar, A.; Saeed, Z.; Rashid, A. Synthesis, spectral and antimicrobial studies of amino acid derivative Schiff base metal (Co, Mn, Cu, and Cd) complexes. *Spectrochim. Acta Part A Mol. Biomol. Spectrosc.* **2019**, *206*, 642–649.
5. Eustathopoulos, N.; Nicholas, M.G.; Drevet, B. (Eds.) *Wettability at High Temperatures*; Elsevier Science Ltd.: Kidlington, UK, 1999; Volume 3.
6. Huang, Z.K.; Liu, H.; Liu, G.W.; Wang, T.T.; Zhang, X.Z.; Wu, J.; Wan, Y.G.; Qiao, G.J. Influences of surface polarity and Pd ion implantation on the wettability of Al-12Si(-2Mg)/SiC systems. *Mater. Chem. Phys.* **2018**, *211*, 329–334.
7. Song, Y.Y.; Liu, D.; Hu, S.P.; Song, X.G.; Lei, Y.Z.; Cao, J. Brazing of metallized SiC ceramic to GH99 superalloy using graphene nanoplatelets reinforced AgCuTi composite filler. *Ceram. Int.* **2019**, *45*, 8962–8970. [[CrossRef](#)]
8. Kashif, M.; Ngaini, Z.; Harry, A.V.; Vekariya, R.L.; Ahmad, A.; Zuo, Z.; Alarifi, A. An experimental and DFT study on novel dyes incorporated with natural dyes on titanium dioxide (TiO<sub>2</sub>) towards solar cell application. *Appl. Phys.* **2020**, *126*, 1–13. [[CrossRef](#)]
9. Barlak, M.; Piekoszewski, J.; Sartowska, B.; Waliś, L.; Starosta, W.; Kierzek, J.; Pochrybniak, C.; Kowalska, E. Wettability of carbon and silicon carbide ceramics induced by their surface alloying with Zr and Cu elements using high intensity pulsed plasma beams. *Nukleonika* **2012**, *57*, 477–483.
10. McCafferty, E. Effect of Ion Implantation on the Corrosion Behavior of Iron, Stainless Steels, and Aluminum—A Review. *Corrosion* **2001**, *57*, 1011–1029. [[CrossRef](#)]
11. Zhao, S.T.; Valenza, F.; Liu, G.W.; Muolo, M.L.; Qiao, G.J.; Passerone, A. Surface characterization of Mo-implanted 6H-SiC by high temperature non-reactive wetting tests with the Ni-56Si alloy. *Ceram. Int.* **2014**, *40*, 7227–7234. [[CrossRef](#)]
12. Huang, Z.K.; Xu, W.L.; Liu, G.W.; Wang, T.T.; Zhang, X.Z.; Qiao, G.J. Wetting and interfacial behavior of molten Al-Si alloys on SiC monocrystal substrates: Effects of Cu or Zn addition and Pd ion implantation. *J. Mater. Sci. Mater. Electron.* **2018**, *29*, 17416–17424. [[CrossRef](#)]
13. Zhu, Y.L.; Zhang, M.F.; Zhang, X.Z.; Huang, Z.K.; Liu, G.W.; Qiao, G.J. Wetting and interfacial behavior of Cu–Al/SiC systems: Influences of Si ion implantation and Al concentration. *J. Alloys Compd.* **2020**, *824*, 153972. [[CrossRef](#)]
14. Fu, W.; Song, X.G.; Tian, R.C.; Lei, Y.Z.; Long, W.M.; Zhong, S.J.; Feng, J.C. Wettability and joining of SiC by Sn-Ti: Microstructure and mechanical properties. *J. Mater. Sci. Technol.* **2020**, *40*, 15–23. [[CrossRef](#)]
15. Yang, J.; Huang, J.H.; Ye, Z.; Chen, S.H.; Ji, R.; Zhao, Y. Influence of interfacial reaction on reactive wettability of molten Ag-Cu-X wt.%Ti filler metal on SiC ceramic substrate and mechanism analysis. *Appl. Surf. Sci.* **2018**, *436*, 768–778. [[CrossRef](#)]
16. Hussain, S.; Yang, X.; Aslam, M.K.; Shaheen, A.; Javed, M.S.; Aslam, N.; Qiao, G. Robust TiN nanoparticles polysulfide anchor for Li-S storage and diffusion pathways using first principle calculations. *Chem. Eng. J.* **2020**, *391*, 123595.
17. Wang, T.T.; Yang, Y.; Ren, Y.B.; Zhu, D.Y.; Zhang, T. Reactive wetting of Ni-Si alloys on graphite substrates: Effects of Si and Ni. *RSC Adv.* **2015**, *5*, 90866–90870. [[CrossRef](#)]
18. Rado, C.; Drevet, B.; Eustathopoulos, N. The role of compound formation in reactive wetting: The Cu/SiC system. *Acta Mater.* **2000**, *48*, 4483–4491. [[CrossRef](#)]
19. Zhou, B.F.; Wang, J.F.; Feng, K.Q. Study on the wetting interface of Zr-Cu alloys on the SiC ceramic surface. *RSC Adv.* **2020**, *10*, 3487–3492. [[CrossRef](#)]
20. Sarafraz, M.M.; Safaei, M.R.; Goodarzi, M.; Yang, B.; Arjomandi, M. Heat transfer analysis of Ga-In-Sn in a compact heat exchanger equipped with straight micro-passages. *Int. J. Heat Mass Transf.* **2019**, *139*, 675–684. [[CrossRef](#)]

21. Sarafraz, M.M.; Jafarian, M.; Arjomandi, M.; Nathan, G.J. Potential use of liquid metal oxides for chemical looping gasification: A thermodynamic assessment. *Appl. Energy* **2017**, *195*, 702–712. [[CrossRef](#)]
22. Sarafraz, M.M.; Tran, N.N.; Pourali, N.; Rebrov, E.V.; Hessel, V. Thermodynamic potential of a novel plasma-assisted sustainable process for co-production of ammonia and hydrogen with liquid metals. *Energy Convers. Manag.* **2020**, *210*, 112709. [[CrossRef](#)]
23. Okamoto, H. Supplemental Literature Review of Binary Phase Diagrams: Ag-Ho, Ag-Tb, Ag-Y, Cd-Na, Ce-Sn, Co-Dy, Cu-Dy, Cu-Sn, Ir-Pt, Mg-Pb, Mo-Ni, and Sc-Y. *J. Phase Equilibria Diffus.* **2014**, *35*, 208–219. [[CrossRef](#)]
24. Amore, S.; Ricci, E.; Lanata, T.; Novakovic, R. Surface tension and wetting behaviour of molten Cu–Sn alloys. *J. Alloys Compd.* **2008**, *452*, 161–166. [[CrossRef](#)]
25. Okamoto, H. Supplemental literature review of binary phase diagrams: Ag-Ni, Ag-Zr, Au-Bi, B-Ni, Co-Sb, Cu-Mn, Cu-Si, Cu-Zn, Fe-Zr, Li-Sb, Mg-Pu, and Si-Zr. *J. Phase Equilibria Diffus.* **2018**, *39*, 87–100. [[CrossRef](#)]
26. Eustathopoulos, N. Progress in understanding and modeling reactive wetting of metals on ceramics. *Curr. Opin. Solid State Mater. Sci.* **2005**, *9*, 152–160. [[CrossRef](#)]
27. Eustathopoulos, N. Wetting by liquid metals—Application in materials processing: The contribution of the grenoble group. *Metals* **2015**, *5*, 350–370. [[CrossRef](#)]



© 2020 by the authors. Licensee MDPI, Basel, Switzerland. This article is an open access article distributed under the terms and conditions of the Creative Commons Attribution (CC BY) license (<http://creativecommons.org/licenses/by/4.0/>).